General theory of the topological Hall effect in systems with chiral spin textures

K. S. Denisov,[1,2,*] I. V. Rozhansky,[1,2] N. S. Averkiev,[1] and E. Lähderanta[2]
[1]*Ioffe Institute, 194021 St. Petersburg, Russia*
[2]*Lappeenranta University of Technology, FI-53851 Lappeenranta, Finland*

(Received 20 July 2018; revised manuscript received 29 October 2018; published 27 November 2018)

We present a consistent theory of the topological Hall effect (THE) in two-dimensional magnetic systems with a disordered array of chiral spin textures, such as magnetic skyrmions. We focus on the scattering regime when the mean-free path of itinerant electrons exceeds the spin texture size, and THE arises from the asymmetric carrier scattering on individual chiral spin textures. We calculate the resistivity tensor on the basis of the Boltzmann kinetic equation taking into account the asymmetric scattering on skyrmions via the collision integral. Our theory describes both the adiabatic regime when THE arises from a spin Hall effect and the nonadiabatic scattering when THE is due to purely charge transverse currents. We analyze the dependence of THE resistivity on a chiral spin texture structure, as well as on material parameters. We discuss the crossover between spin and charge regimes of THE driven by the increase of skyrmion size, the features of THE due to the variation of the Fermi energy, and the exchange interaction strength; we comment on the sign and magnitude of THE.

DOI: 10.1103/PhysRevB.98.195439

I. INTRODUCTION

Among rich variety of transport phenomena in magnetic materials the special attention is now focused on the topological Hall effect (THE). THE is the appearance of an additional transverse voltage due to itinerant carrier exchange interaction with chiral spin textures, such as magnetic skyrmions [1–4]. During the recent extensive experimental studies the detection of THE signal has proved itself as an indicator that a sample magnetization acquires a chiral structure. The observation of THE has been reported for various systems exhibiting different chiral ordering of spins: skyrmion crystals [5–8], antiferromagnets (AFM) [9,10], spin glasses [11,12], and arrays of magnetic skyrmions [13–21].

Naturally, an appropriate microscopic theory of THE has to take into account the particular type of chiral spin ordering. In the case of a regular noncollinear spin structure with periodic or quasiperiodic spin arrangement [22–24], such as AFM lattices [9] or skyrmion crystals [6,25,26], THE is usually described via the mean-field approach and using the adiabatic approximation [6,22,27]. The adiabatic theory is based on the geometric Berry phase interpreted as an effective magnetic field acting on an electron. Although the Berry phase description of THE has been widely applied for various systems [28–35], it is, however, invalid for a weak exchange coupling [36,37]. The latter case has been recently studied using different theoretical methods [38–42].

Another class of chiral spin systems studied experimentally is a disordered array of localized small chiral spin textures such as magnetic skyrmions [14–16,20,43]. The description of THE in terms of an effective mean magnetic field fails in this case as there is no regular long-range chiral spin structure which can be described by a homogeneous effective magnetic field. On the contrary, a carrier moves freely most of the time with an occasional scattering on localized magnetization vortices. The important feature of the individual scattering regime is that the properties of THE strongly depend on whether the carrier spin-flip processes are activated or not corresponding to weak coupling regime and adiabatic regime, respectively [44]. The transverse electric response arises from the spin Hall effect [22,34] in the adiabatic regime and from the charge Hall effect in the weak coupling regime [38,41]. Thus, the complete theory of THE for the irregular dilute chiral systems requires an accurate treatment of carrier scattering on a single chiral spin texture.

In this paper we develop the theory of the topological Hall effect in disordered systems of chiral spin textures. We consider a two-dimensional (2D) metal with both electron spin subbands populated when THE can be generated either by charge or by spin transverse currents. Our approach is based on the calculation of the exact scattering parameters on individual spin textures presented in Ref. [44]. The paper is organized as follows: in Sec. II the kinetic theory of THE is described accounting for the carrier scattering on host impurities and noncollinear spin textures, in Sec. III the properties of the exchange asymmetric scattering are discussed, Sec. IV covers the dependence of THE on material and spin texture parameters, we also describe the crossover between charge and spin Hall regimes of THE driven by the suppression of spin-flip scattering; in Sec. V we discuss the obtained results in the view of some real skyrmion systems.

II. KINETIC THEORY

Let us consider two-dimensional degenerate electron gas (2DEG) described by the Hamiltonian:

$$\mathcal{H} = \frac{p^2}{2m} - \alpha_0 \boldsymbol{S}(\boldsymbol{r}) \cdot \boldsymbol{\sigma} + \sum_i u(\boldsymbol{r} - \boldsymbol{r}_i), \quad (1)$$

*denisokonstantin@gmail.com

where the first term describes the electron free motion with an effective in-plane mass m, the second term represents the electron exchange interaction with a magnetic texture described by a static spin field $\boldsymbol{S}(\boldsymbol{r})$, where α_0 is an exchange coupling constant, $\boldsymbol{\sigma}$ is the vector of Pauli matrices, and the last term describes scattering on host nonmagnetic impurities located at $\boldsymbol{r}_i$. The topological Hall effect appears when $\boldsymbol{S}(\boldsymbol{r})$ has a noncollinear structure characterized by a nonzero spin chirality.

We consider the case, when the spin field $\boldsymbol{S}(\boldsymbol{r})$ consists of two contributions:

$$\boldsymbol{S}(\boldsymbol{r}) = S_0\boldsymbol{e}_z + \sum_j \delta\boldsymbol{S}(\boldsymbol{r}-\boldsymbol{r}_j). \tag{2}$$

The first term is a background homogeneous field directed perpendicular to the 2DEG plane leading to the spin splitting $\Delta = \alpha_0 S_0$, we assume ferromagnetic exchange interaction ($\Delta > 0$). The energy dispersion for the two spin branches $s = \pm 1/2$ is $\varepsilon_p^s = p^2/2m - s\Delta$; the spin-dependent velocity is given by $v_s = \sqrt{2(\varepsilon + s\Delta)/m}$, where ε is the electron energy. We further assume that the Fermi energy E_F exceeds the spin splitting so that both spin subbands are populated ($E_F > \Delta/2$). The second contribution in Eq. (2) describes localized chiral spin textures $\delta\boldsymbol{S}$ of a few nanometer size located at $\boldsymbol{r}_j$ and causing an additional elastic scattering of the carriers. While magnetic skyrmions are the typical example of such spin texture, our consideration covers a much wider class of chiral spin textures, not necessarily having a nonzero topological charge [44]. The feature of the chiral spin structures is that for a given incident electron flux there is a difference in scattering rates to the left and to the right, eventually leading to the Hall effect.

We consider the classic transport regime ($k_F\ell \gg 1$, where $k_F = \sqrt{2mE_F}/\hbar$ is the Fermi wave vector, and ℓ is the mean free path) on the basis of the Boltzmann kinetic equation:

$$e\boldsymbol{E}\cdot\frac{\partial f_s(\boldsymbol{p})}{\partial \boldsymbol{p}} = \mathrm{St}[f_s(\boldsymbol{p})],$$
$$\mathrm{St}[f_s(\boldsymbol{p})] = \sum_{\boldsymbol{p}',s'}\left(\mathcal{W}_{\boldsymbol{p}\boldsymbol{p}'}^{ss'} f_{s'}(\boldsymbol{p}') - \mathcal{W}_{\boldsymbol{p}'\boldsymbol{p}}^{s's} f_s(\boldsymbol{p})\right), \tag{3}$$

where $f_s(\boldsymbol{p})$ is the distribution function, $\boldsymbol{p}$ is 2D momentum, and $s = \pm 1/2$ is the carrier spin projection on the axis normal to the motion plane, $\boldsymbol{E}$ is an in-plane electric field, $\mathcal{W}_{\boldsymbol{p}\boldsymbol{p}'}^{ss'}$ is the elastic scattering rate from $(\boldsymbol{p}', s')$ to $(\boldsymbol{p}, s)$ state, and e is the electron charge. We solve Eq. (3) in linear approximation with respect to $\boldsymbol{E}$.

Expressing the scattering rate $\mathcal{W}_{\boldsymbol{p}\boldsymbol{p}'}^{ss'}$ in the form of the Fermi's golden rule we assume that it has two contributions:

$$\mathcal{W}_{\boldsymbol{p}\boldsymbol{p}'}^{ss'} = \frac{2\pi}{\hbar}\left(n_i|u_{\boldsymbol{p}\boldsymbol{p}'}|^2\delta_{ss'} + n_{\mathrm{sk}}\left|T_{\boldsymbol{p}\boldsymbol{p}'}^{ss'}\right|^2\right)\delta\left(\varepsilon_p^s - \varepsilon_{p'}^{s'}\right), \tag{4}$$

where the first term in parentheses describes the electron spin-independent scattering on nonmagnetic impurities, and the second term is driven by the scattering on chiral spin textures; interference effects between the two types of scatterers are neglected. Here n_i, n_{sk} are the surface densities of impurities and localized magnetic textures, respectively, $u_{\boldsymbol{p}\boldsymbol{p}'}$ is Fourier transform of the nonmagnetic impurity potential $u(\boldsymbol{r})$ from Eq. (1), $T_{\boldsymbol{p}\boldsymbol{p}'}^{ss'}$ is the exact T matrix of electron scattering on the spin texture, and the delta function ensures energy conservation in the elastic scattering. Two contributions can be distinguished in the square modulus of the T matrix:

$$\nu^2\left|T_{\boldsymbol{p}\boldsymbol{p}'}^{ss'}\right|^2 = \mathcal{G}_{ss'}(\theta) + \mathcal{J}_{ss'}(\theta),$$
$$\mathcal{G}_{ss'}(\theta) = \mathcal{G}_{ss'}(-\theta), \quad \mathcal{J}_{ss'}(\theta) = -\mathcal{J}_{ss'}(-\theta). \tag{5}$$

$\mathcal{G}_{ss'}(\theta)$, $\mathcal{J}_{ss'}(\theta)$ are dimensionless symmetric and asymmetric scattering rates, respectively, $\theta = \varphi - \varphi'$ is the scattering angle, φ, φ' are the polar angles of $\boldsymbol{p}$, $\boldsymbol{p}'$, and $\nu = m/2\pi\hbar^2$ is the 2D density of states (per one spin). In the introduced notation we omit the dependence of $\mathcal{G}_{ss'}$, $\mathcal{J}_{ss'}$ on the electron energy ε.

It is the asymmetric part $\mathcal{J}_{ss'}(\theta)$ of an electron scattering on chiral spin textures that gives rise to the transversal current as the scattering rates to the left and to the right become unequal. The scattering asymmetry acts as an effective magnetic field, which sign can be either the same for both spin projections of an incident electron, hence leading to a charge Hall effect, or opposite for the opposite electron spin projections, leading to the spin Hall effect. The properties of $\mathcal{J}_{ss'}(\theta)$ are discussed in Ref. [44] and summarized in Sec. III.

The distribution function $f_s(\boldsymbol{p}) = f_s^0(\varepsilon) + g_s(\boldsymbol{p})$ contains equilibrium $f_s^0(\varepsilon)$ and nonequilibrium $g_s(\boldsymbol{p})$ parts; the latter describes the appearance of the electric current in an external electric field $\boldsymbol{E}$. Below the direction of $\boldsymbol{E}$ is assumed along x axis, and the polar angle φ of momentum $\boldsymbol{p}$ is counted from x axis. In order to solve the kinetic equation (3) one should expand $g_s(\boldsymbol{p})$ and $\mathcal{W}_{\boldsymbol{p}\boldsymbol{p}'}^{ss'}$ in a series of angular harmonics $\cos n\varphi$, $\sin n\varphi$ and perform the integration over the angle φ' in the collision integral. The details of this calculation are given in Appendix A.

In this paper we focus on the linear regime in $\boldsymbol{E}$, so g_s contains only first angular harmonics:

$$g_s(\boldsymbol{p}) = g_s^+\cos\varphi + g_s^-\sin\varphi. \tag{6}$$

The terms g_s^+, g_s^- determine the longitudinal and transverse electric currents, respectively. Indeed, as $\boldsymbol{E}$ is along x axis, we get for the electric current $\boldsymbol{j}$:

$$\begin{pmatrix} j_x \\ j_y \end{pmatrix} = e\sum_{\boldsymbol{p},s} g_s(\boldsymbol{p}) v \begin{pmatrix} \cos\varphi \\ \sin\varphi \end{pmatrix}$$
$$= e\frac{\nu}{2}\sum_s \int v_s(\varepsilon)d\varepsilon \begin{pmatrix} g_s^+(\varepsilon) \\ g_s^-(\varepsilon) \end{pmatrix}, \tag{7}$$

where the integration goes over the energy ε. The topological Hall effect related to the transverse electric current j_y is thus determined by g_s^- coefficients. The explicit integration of the collision integral in Eq. (3) over $\boldsymbol{p}'$ brings us to the following system of equations on $g_s^\pm$ (see details in Appendix A):

$$eE\begin{pmatrix} v_\uparrow \frac{\partial f_\uparrow^0}{\partial \varepsilon} \\ 0 \\ v_\downarrow \frac{\partial f_\downarrow^0}{\partial \varepsilon} \\ 0 \end{pmatrix} = \begin{pmatrix} -\tau_\uparrow^{-1} & \Omega_{\uparrow\uparrow} & \tau_{\uparrow\downarrow}^{-1} & \Omega_{\uparrow\downarrow} \\ -\Omega_{\uparrow\uparrow} & -\tau_\uparrow^{-1} & -\Omega_{\uparrow\downarrow} & \tau_{\uparrow\downarrow}^{-1} \\ \tau_{\downarrow\uparrow}^{-1} & \Omega_{\downarrow\uparrow} & -\tau_\downarrow^{-1} & \Omega_{\downarrow\downarrow} \\ -\Omega_{\downarrow\uparrow} & \tau_{\downarrow\uparrow}^{-1} & -\Omega_{\downarrow\downarrow} & -\tau_\downarrow^{-1} \end{pmatrix} \begin{pmatrix} g_\uparrow^+ \\ g_\uparrow^- \\ g_\downarrow^+ \\ g_\downarrow^- \end{pmatrix}. \tag{8}$$

Here we introduced the following parameters:

$$\begin{aligned}
&\tau_s^{-1} = \tau_0^{-1} + \omega_s, \quad \tau_0^{-1} = n_i \frac{2\pi}{\hbar}\nu \int_0^{2\pi} |u_{\boldsymbol{pp}'}|^2 (1-\cos\theta)\frac{d\theta}{2\pi},\\
&\omega_s = n_{\rm sk}\frac{2\pi}{\hbar}\int_0^{2\pi} [(1-\cos\theta)\mathcal{G}_{ss}(\theta) + \mathcal{G}_{\bar{s}s}]\frac{1}{\nu}\frac{d\theta}{2\pi},\\
&\tau_{s\bar{s}}^{-1} = n_{\rm sk}\frac{2\pi}{\hbar}\int_0^{2\pi} \mathcal{G}_{s\bar{s}}(\theta)\cos\theta \frac{1}{\nu}\frac{d\theta}{2\pi},\\
&\Omega_{ss'} = \frac{eB_{ss'}}{mc}, \quad B_{ss'} = (n_{\rm sk}\phi_0)\int_0^{2\pi} \mathcal{J}_{ss'}(\theta)\sin\theta d\theta,
\end{aligned} \tag{9}$$

where τ_s is the total transport lifetime, τ_0 is the transport lifetime for the scattering on nonmagnetic impurities, and ω_s^{-1} and $\tau_{s\bar{s}}$ are the transport lifetimes for the scattering on chiral textures (here $\bar{s}$ is the spin subband index opposite to s). The transverse Hall current due to the asymmetric scattering is driven by $\Omega_{ss'}$, which is analogous to the cyclotron frequency in the ordinary Hall effect; $B_{ss'}$ is the corresponding effective magnetic field, $\phi_0 = hc/|e|$ is the magnetic flux quantum, and c is the speed of light. Solving the system Eq. (8) and finding $g_s^{\pm}$ allow us to calculate the resistivity tensor ρ for various transport scenarios as further discussed in Sec. IV. We would like to emphasize that both spin-conserving and spin-flip scattering channels contain asymmetric parts $\Omega_{ss'}$ and thus contribute to g_s^- and j_y.

III. ASYMMETRIC ELECTRON SCATTERING ON A CHIRAL SPIN TEXTURE

In this section we consider the features of asymmetric electron scattering on a single chiral magnetic texture. We express the scattering potential in the form

$$V(\boldsymbol{r}) = -\alpha_0 \delta\boldsymbol{S}(\boldsymbol{r})\cdot\boldsymbol{\sigma}. \tag{10}$$

Outside the localized spin texture of a characteristic diameter a the magnetization is unperturbed so that $\delta\boldsymbol{S}(r > a/2) \to 0$ and the scattering potential vanishes. The topological Hall effect appears due to the asymmetry in the electron scattering when the potential (10) can be characterized by a nonzero chirality. The details of the asymmetric scattering depend on the particular distribution of spins in the texture and its size as well as on the exchange interaction strength and the incident electron wavevector [44].

A. Chiral spin textures

To describe a chiral spin texture in 2D the following parametrization is commonly used:

$$\delta\boldsymbol{S}(\boldsymbol{r}) = \begin{pmatrix} \delta S_\parallel(r)\cos(\varkappa\phi+\gamma)\\ \delta S_\parallel(r)\sin(\varkappa\phi+\gamma)\\ \delta S_z(r)\end{pmatrix}, \tag{11}$$

where $\boldsymbol{r} = (r,\phi)$ is the polar radius vector, and $r = 0$ corresponds to the center of the texture. The functions $\delta S_\parallel, \delta S_z \neq 0$ depend on the distance from the center r. The vorticity $\varkappa$ describes the in-plane spin rotation with an initial phase γ. In what follows we consider that δS_z is counted from the background magnetization S_0, whose sign we denote as $\eta = \mathrm{sgn}(S_0)$. In the last section we will also consider the case when S_0 and δS_z are independent.

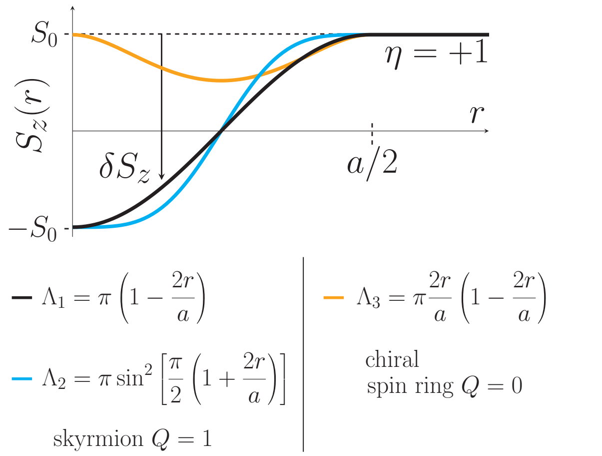

FIG. 1. The typical profiles $S_z(r) = S_0\cos\Lambda(r)$ of chiral spin textures. Note that for $\eta = +1$, the $\delta S_z(r) < 0$ is negative.

Figure 1 shows the profiles $S_z(r) = S_0\cos\Lambda(r)$ for three examples of chiral spin textures with $\eta = +1$ (we assume that $\delta S_\parallel^2 = S_0^2 - S_z^2$). Two of them describe a magnetic skyrmion ($\Lambda_1(r) = \pi(1-2r/a)$, $\Lambda_2(r) = \pi\sin^2[(\pi/2)(1+2r/a)]$). The skyrmion has an opposite sign of spins in its center with respect to the background magnetization, which leads to the appearance of a nonzero topological charge called winding number Q. The nonzero Q is particularly important for the thermal stability of skyrmions in ferromagnetic thin films [45–52]. The third magnetization profile Fig. 1 [$\Lambda_3(r) = (2r/a)\pi(1-2r/a)$] corresponds to a chiral spin ring with the orientation of spins in the center parallel to S_0. Chiral rings have zero winding number, but they exhibit a similar topological Hall effect [44]. Such spin textures can appear in a material with spin-orbit interaction functionalized by magnetic impurities, in a vicinity of a defect or impurity [53–56]. Let us notice that for the positive background spin orientation ($\eta = +1$) δS_z is negative.

Substituting (11) into (10) we get for the scattering potential:

$$V(\boldsymbol{r}) = -\alpha_0\begin{pmatrix} \delta S_z(r) & e^{-i\varkappa\phi - i\gamma}\delta S_\parallel(r)\\ e^{i\varkappa\phi+i\gamma}\delta S_\parallel(r) & -\delta S_z(r)\end{pmatrix}. \tag{12}$$

The potential $V(\boldsymbol{r})$ is a 2×2 matrix, which depends on a polar angle ϕ via the off-diagonal components. When both functions S_z, $S_\parallel$ are nonzero, the angular dependence of the potential leads to the appearance of the asymmetric part in electron scattering rates $\mathcal{J}_{ss'}(\theta) = -\mathcal{J}_{ss'}(-\theta)$, where θ is the scattering angle. The sign of $\mathcal{J}_{ss'}$ depends on $\varkappa$. The phase parameter γ is an important characteristic of a skyrmion structure, i.e., $\gamma = \pi/2$, $\gamma = 0$ correspond to Bloch and Néel skyrmions, respectively. However, γ does not affect the scattering cross section and, therefore, appears to play no role in THE. The role of η is more complicated; we further explicitly specify the dependence of $\mathcal{J}_{ss'}(\theta,\eta)$ on η.

B. Asymmetric scattering features

We consider the case when Fermi energy exceeds the background exchange splitting $E_F > \Delta/2$ so that both spin subbands are populated with electrons ($\Delta = \alpha_0 S_0$). The symmetry upon the time inversion allows us to present the asymmetric scattering rates $\mathcal{J}_{ss'}(\theta,\eta)$ introduced in Eq. (5) in the form (see the details in Appendix B)

$$\begin{aligned}\mathcal{J}_{\uparrow\uparrow}(\theta,\eta)&=\eta\Gamma_1(\theta)+\Pi(\theta),\\ \mathcal{J}_{\downarrow\downarrow}(\theta,\eta)&=\eta\Gamma_1(\theta)-\Pi(\theta),\\ \mathcal{J}_{\uparrow\downarrow}(\theta,\eta)&=\mathcal{J}_{\downarrow\uparrow}(\theta,\eta)=\eta\Gamma_2(\theta),\end{aligned}\tag{13}$$

where $\Gamma_{1,2}(\theta)$ and $\Pi(\theta)$ have no dependence on the background polarization $\eta=\mathrm{sgn}(S_0)$. This representation is convenient for treating the topological charge and spin Hall effects independently. Indeed, the terms $\eta\Gamma_{1,2}$ describe the asymmetric scattering in the same transverse direction determined by the texture orientation η and independent of an initial carrier spin state. These terms, therefore, lead to the charge Hall effect. On the contrary, the term Π describes the scattering of spin up and spin down electron in the opposite transverse directions independent of η. This process leads to spin Hall effect, it is absent for spin-flip channels. Both $\Gamma_{1,2}$ and Π change their sign upon $\varkappa\to-\varkappa$.

Which of the two contributions to the topological Hall effect (charge or spin) dominate strongly depends on whether the spin-flip processes are activated or not. Away from the threshold $E_F\gg\Delta/2$ the rate of the spin-flip scattering is controlled by the adiabatic parameter $\lambda_a=(\alpha_0S_0/\hbar)\tau_a$, where $\tau_a=a/v_F$ is an electron time of flight through the texture of diameter a with Fermi velocity $v_F=\sqrt{2E_F/m}$.

In the case of $\lambda_a\leqslant1$ the spin-flip processes are effective, the asymmetric scattering arises from the interference between double spin-flip and single spin-conserving scattering events (so-called spin-chirality driven mechanism [36,37,39,41,42]). This process is sensitive to the spin chirality χ defined for any three spins $\delta\boldsymbol{S}_1,\delta\boldsymbol{S}_2,\delta\boldsymbol{S}_3$ forming the spin texture as $\chi=(\delta\boldsymbol{S}_1\cdot[\delta\boldsymbol{S}_2\times\delta\boldsymbol{S}_3])$. The nonzero chirality of the spin texture in the weak coupling regime leads to the charge Hall effect. The spin chirality based contribution is described by $\Gamma_{1,2}$. At $\lambda_a\leqslant1$ these terms dominate $\Gamma_{1,2}\gg\Pi$, with spin-flip scattering prevailing $\Gamma_2=2\Gamma_1$.

In the opposite case of large adiabatic parameter $\lambda_a\gg1$ the spin-flip processes are suppressed in accordance with the adiabatic theorem. In this regime the scattering asymmetry is due to the Berry phase acquired by the wave function of the electron moving through a noncollinear spin field in the real space. The hallmark of this mechanism is that the sign of the effective magnetic field associated with the Berry phase appears to be opposite for spin up and spin down electrons, thus leading to the spin Hall effect [22,30,32,33]. This adiabatic contribution to the Hall response is, therefore, described by Π. At $\lambda_a\gg1$ the spin Hall effect dominates $\Pi\gg\Gamma_{1,2}$, and the charge Hall effect appears only due to nonzero carrier spin polarization P_s.

The interplay between charge and spin topological Hall effects leads to a few nontrivial features discussed in the following section.

IV. TOPOLOGICAL HALL EFFECT

In this section we discuss the topological contribution to the Hall resistivity ρ_{yx}^T in the diffusive regime for different systems.

A. Dilute array of chiral spin textures

Let us consider a two-dimensional film containing spatially localized chiral spin textures such as magnetic skyrmions or chiral magnetic rings (see Fig. 1). We assume that all the textures have the same vorticity $\varkappa$, and the orientation $\eta=\mathrm{sgn}(S_0)=+1$ is fixed, being determined by the background magnetization S_0. We consider the dilute regime, when the scattering rate on spin textures is much smaller than that on nonmagnetic impurities $\omega_s\tau_0\ll1$, $\Omega_{ss'}\tau_0\ll1$, so the transport lifetime is given by $\tau_s=\tau_0$. Solving the system (8) for $g_s^{\pm}$ in the lowest order in $(\Omega_{ss'}\tau_0)$ we express the topological Hall resistivity ρ_{yx}^T as a sum of two contributions (see details in Appendix C):

$$\begin{aligned}\rho_{yx}^T&=\rho_c+\rho_a,\\ \rho_c&=\frac{1}{nec}(\phi_0n_{\mathrm{sk}})\int_0^{2\pi}(\Gamma_1+\Gamma_2)\sin\theta d\theta,\\ \rho_a&=P_s\frac{1}{nec}(\phi_0n_{\mathrm{sk}})\int_0^{2\pi}\Pi\sin\theta d\theta.\end{aligned}\tag{14}$$

The term ρ_c describes the charge transverse current (charge Hall effect) generated due to carrier asymmetric scattering due to spin-independent terms $\Gamma_{1,2}$ [Eq. (13)]. The term ρ_a describes the transverse spin current (spin Hall effect) driven by the spin-dependent contribution to the asymmetric scattering Π [Eq. (13)]. The spin current does not lead to a charge separation unless there is unequal number of spin up and spin down carriers in the system. Therefore, this contribution to the Hall resistivity is proportional to the carrier spin polarization $P_s=(n_\uparrow-n_\downarrow)/(n_\uparrow+n_\downarrow)=\Delta/2E_F$. In Eq. (14) the notation $n=n_\uparrow+n_\downarrow$ stands for the 2DEG sheet density.

The relative importance of the two contributions ρ_a and ρ_c in the appearance of the transverse charge current depends on the texture diameter a or the Fermi level E_F as discussed in the following sections.

1. Crossover between charge and spin Hall effect

Let us trace the dependence of ρ_{yx}^T (14) on the spin texture diameter a. We assume that the Fermi energy E_F substantially exceeds the exchange spin splitting so that both spin subbands are populated and the spin polarization of the carriers is far below 100%: $P_s=\Delta/2E_F\ll1$. The adiabatic parameter can be expressed as $\lambda_a=P_s(ka)$, where $k=\sqrt{2E_Fm/\hbar^2}$. Figure 2 shows the calculated dependence of charge ρ_c, adiabatic ρ_a, and total ρ_{yx}^T Hall resistivities on the skyrmion diameter a for the magnetic skyrmion with magnetization spatial profile $\Lambda_1(r)$ shown in Fig. 1. For the calculation results shown in Fig. 2 the spin polarization was taken $P_s=0.4$, and the skyrmion surface density $n_{\mathrm{sk}}=2\times10^{11}$ cm^{-2}. The scattering rates $\mathcal{J}_{ss'}$ were calculated using the phase function method [44]. As can be seen in Fig. 2, for $\lambda_a\leqslant1.8$ the charge contribution ρ_c exceeds ρ_a, at that ρ_{yx}^T is dominated by the purely charge current. For $\lambda_a\geqslant4.5$ the adiabatic term prevails $\rho_a\gg\rho_c$ and ρ_{yx}^T appears due to the spin current converted into the charge current. In addition to the adiabatic parameter, the change of the texture size at the same time affects the wave parameter ka, which determines the properties of the scattering. As a result, the topological Hall resistivity ρ_{yx}^T

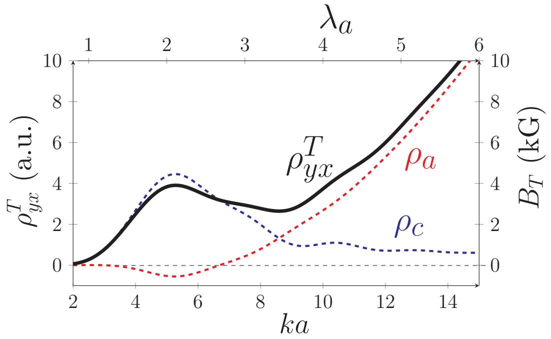

FIG. 2. The dependence of ρ_{yx}^T on magnetic skyrmion diameter ka for Λ_1 profile, and the crossover between charge and spin topological Hall effects. The parameters $P_s = 0.4$, $n_{\rm sk} = 2 \times 10^{11}$ cm^{-2}.

exhibits a nontrivial dependence on a in the intermediate region $4.5 \gtrsim \lambda_a \gtrsim 1.8$. As the spin-flip processes become suppressed, first the charge contribution ρ_c is decreased, and only later the adiabatic term ρ_a starts to increase. This effect results in the appearance of the local minimum for ρ_{yx}^T in the crossover regime.

The behavior of ρ_{yx}^T in the crossover regime is highly sensitive to a particular magnetic texture profile. In Fig. 3 we present the dependence of ρ_{yx}^T on a for three different spin texture spatial profiles shown in Fig. 1. As can be seen in Fig. 3 the oscillating structure of ρ_{yx}^T upon increasing ka exhibits a significant variation even for two very similar skyrmion configurations Λ_1 and Λ_2. The strong dependence of ρ_{yx}^T on $\Lambda(r)$ observed in the crossover regime is due to the significance of the interference in electron scattering as the wave parameter $ka \sim \pi$ [44]. The texture described by Λ_2 has larger spin gradients, so the adiabatic term activates at larger ka, and the magnitude of ρ_{yx}^T for Λ_2 in the crossover regime is smaller than that of Λ_1.

We would also like to stress out that the topological Hall effect exists as well due to scattering on chiral spin rings having zero winding number (orange curve in Fig. 3). The transverse conductivity ρ_{yx}^T due to scattering on chiral spin rings possesses all the features described above including the the existence of charge and spin Hall limiting regimes.

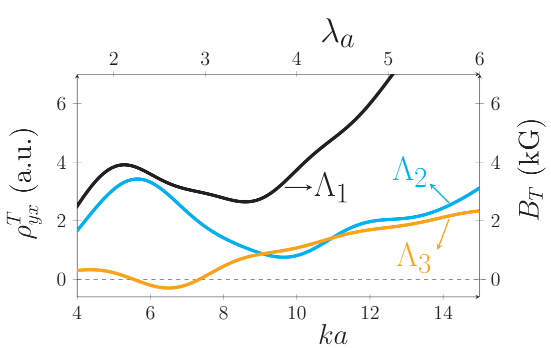

FIG. 3. The dependence of ρ_{yx}^T on chiral texture diameter ka for different texture profiles in the region of crossover. The parameters $P_s = 0.4$, $n_{\rm sk} = 2 \times 10^{11}$ cm^{-2}.

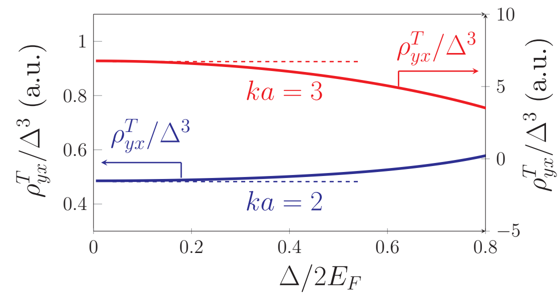

FIG. 4. The dependence of ρ_{yx}^T/Δ^3 on the variation of $\Delta/2E_F$ at $ka = 2$ (blue curve) and $ka = 3$ (red curve) for Λ_1 profile.

2. The magnitude of the topological Hall effect

The magnitude of THE for the dilute systems can be expressed in terms of the effective magnetic field B_T introduced as

$$\rho_{yx}^T = \frac{B_T}{nec},$$
$$B_T = (\phi_0 n_{\rm sk}) \int_0^{2\pi} (\Gamma_1 + \Gamma_2 + P_s \Pi) \sin\theta d\theta. \quad (15)$$

The field B_T shows the magnitude of the external magnetic field applied to the sample, at which the ordinary Hall effect contribution to the transverse resistivity $\rho_{yx}^{\mathcal{O}}$ becomes comparable with ρ_{yx}^T.

Usually in the THE estimates it is assumed that each skyrmion contributes via a magnetic flux quantum, so that in the adiabatic regime $|B_T| \approx P_s(\phi_0 n_{\rm sk})Q$. However, our analysis shows that such an estimate does not take into account the important features of the scattering. According to Eq. (15), ρ_{yx}^T and B_T linearly depend on both the skyrmion surface density $n_{\rm sk}$ and the dimensionless scattering rates $\Gamma_{1,2}$, Π. Therefore, the magnitude of B_T is renormalized differently depending on the scattering regime.

For instance, in the weak coupling regime ($\lambda_a \leqslant 1$) B_T scales as Δ^3, as the perturbation theory couples $\Gamma_{1,2}$ with spin chirality [36,41] and, therefore, THE requires the third order in the exchange interaction. In Fig. 4 the quantity ρ_{yx}^T/Δ^3 is shown for two values of $ka = 2, 3$. As can be seen from the figure, the scaling Δ^3 holds up to $\Delta/2E_F \approx 0.2$, the deviation from the scaling relation indicates that the perturbation theory becomes invalid departing from the weak coupling regime.

Let us note that although the asymmetrical scattering rates $\Gamma_{1,2}$ are small in the weak coupling regime [$\Gamma_{1,2}$ are proportional to $(\Delta/2E_F)^3(ka/2)^8$ at $\lambda_a < 1$], the magnitude of B_T can be enhanced by increasing $n_{\rm sk}$. For example, for $n_{\rm sk} = 5 \times 10^{12}$ cm^{-2} and $\lambda_a = 0.8$ ($ka = 2$, $P_s = 0.4$) one gets $B_T \approx 0.7$ T.

The magnitude of B_T in the intermediate and strong coupling regimes for $n_{\rm sk} = 2 \times 10^{11}$ cm^{-2} can be seen in Figs. 2 and 3 and Figs. 6 and 7. At $n_{\rm sk}\phi_0 \approx 8$ T the value of B_T in the intermediate regime is of the order of several kG; while in the strong coupling regime ($\lambda_a \gg 1$) it can go as high as several Tesla [57]. It is worth noticing that the conventional estimate $|B_T| \approx P_s(\phi_0 n_{\rm sk})Q$ widely used in the literature is applicable only in the adiabatic limit $\lambda_a \gg 1$ for a large skyrmion size $ka \gg 1$. In Fig. 5 we show the dependence of ρ_{yx}^T on ka for

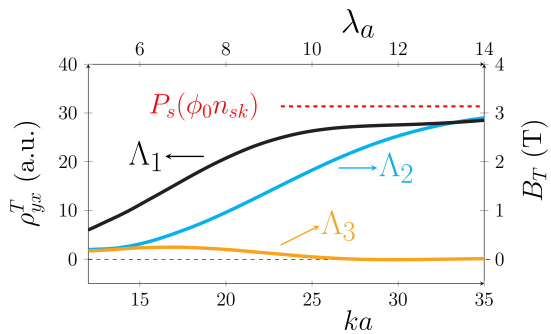

FIG. 5. The dependence of ρ_{yx}^T on chiral texture diameter ka for different texture profiles in the adiabatic region. The parameters $P_s = 0.4$, $n_{\rm sk} = 2 \times 10^{11}$ cm^{-2}. The saturation magnitude $P_s(\phi_0 n_{\rm sk}) \approx 3.3$ T.

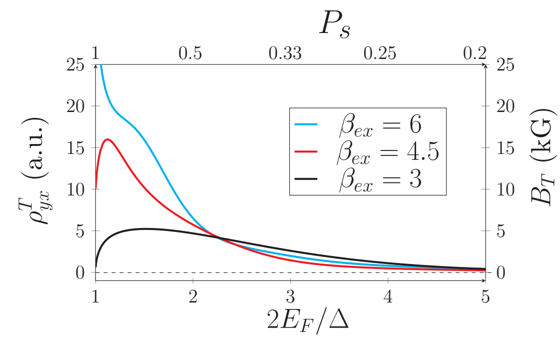

FIG. 6. The dependence of ρ_{yx}^T on Fermi energy E_F at different $\beta_{\rm ex} = \sqrt{m\Delta/\hbar^2}a$ parameter for Λ_1 profile, $n_{\rm sk} = 2 \times 10^{11}$ cm^{-2}.

three texture profiles from Fig. 1 at $ka \gg 1$. Let us mention that B_T starts to saturate at $ka \geqslant 30$ for the textures with nonzero topological charge ($\Lambda_{1,2}$) approaching its maximum value $P_s(\phi_0 n_{\rm sk})$ at $ka \geqslant 35$. On the contrary, THE resistivity asymptotically falls to zero for Λ_3 spin texture having $Q = 0$. Therefore, the topological charge is indeed important for THE in the quasiclassical limit $ka \gg 1$, while in all other cases the local chirality of the spin texture leads to emergence of THE independently of Q.

3. The sign of the topological Hall effect

In a real experiment when electron transport in a system with chiral spin textures is studied as a function of the external magnetic field B_0, it is often difficult to extract different contributions to the Hall effect. The total transverse resistivity ρ_{yx} contains three contributions $\rho_{yx} = \rho_{yx}^{\mathcal{O}} + \rho_{yx}^{\mathcal{A}} + \rho_{yx}^T$, where $\rho_{yx}^{\mathcal{O}}$, $\rho_{yx}^{\mathcal{A}}$, and ρ_{yx}^T are attributed to the ordinary, anomalous, and topological Hall effects, respectively. Here we focus on the sign difference between $\rho_{yx}^T = (B_T/nec)$ and $\rho_{yx}^{\mathcal{O}} = (B_0/nec)$, thus we should compare the signs of B_T and B_0.

We assume that the background magnetization S_0 is directed along the external magnetic field $B_0 > 0$. In general, there is no any fixed relation between the signs of the topological Hall resistivity ρ_{yx}^T, charge ρ_c, and adiabatic ρ_a contributions as can be seen in Fig. 2. In this figure ρ_a changes its sign with increase of ka. For some spin texture profiles the total topological resistivity ρ_{yx}^T can also change its sign in the crossover regime. This is the case for Λ_3 spin configuration as can be seen in Fig. 3. However, it is possible to specify the sign of B_T in the limiting regimes, i.e., away from the threshold $E_F \gg \Delta/2$ and outside the adiabatic crossover $\lambda_a \approx 1$. Let us consider the weak coupling regime ($\lambda_a \leqslant 1$), in which the charge current contribution to THE dominates ($\rho_c \gg \rho_a$). In this regime, the effective magnetic field is proportional to the chirality of the spin texture $B_T \propto \delta \boldsymbol{S}_1 \cdot [\delta \boldsymbol{S}_2 \times \delta \boldsymbol{S}_3]$. For $\varkappa = +1$, $\eta = +1$ the sign of the mixed vector product of any three spins $\delta \boldsymbol{S}_1, \delta \boldsymbol{S}_2, \delta \boldsymbol{S}_3$ forming the skyrmion is negative and $B_T < 0$ due to $\delta S_z < 0$ (see Fig. 1), thus the sign of B_T appears to be opposite to B_0. In the adiabatic regime ($\rho_a \gg \rho_c$) the electrons with positive spin projection (co-aligned with S_0) retain the same type of scattering asymmetry as for small λ_a. As these electrons constitute the majority at a positive spin polarization ($P_s > 0$), the effective magnetic field is also negative $B_T < 0$.

We conclude that for $\varkappa = +1$, $\eta = +1$ configurations, the topological field B_T usually has the opposite sign to the sign of the external field B_0. For chiral spin configurations with negative vorticity $\varkappa < 0$ the fields B_T and B_0 have the same sign. However, in the crossover regime $\lambda_a \sim 1$ and near the threshold $E_F \approx \Delta/2$ there is no any fixed relation between B_0 and B_T signs.

4. Effect of the Fermi energy variation

The dependence of ρ_{yx}^T on the variation of the Fermi energy E_F exhibits a number of distinctive features. At $E_F < \Delta/2$ only one spin subband is occupied and spin polarization is $P_s = 1$. We start the analysis from the threshold $E_F \geqslant \Delta/2$, when the electrons start populating the second spin subband. In further consideration we keep Δ and a constant changing only the Fermi energy E_F. For this analysis it is convenient to combine Δ and a into a single parameter $\beta_{\rm ex} = \lambda_a/\sqrt{P_s} = \sqrt{m\Delta/\hbar^2}a$, which is independent of E_F. Figure 6 shows the dependence of ρ_{yx}^T on E_F calculated for the Λ_1 skyrmion configuration for three different values of $\beta_{\rm ex}$. As can be seen from the figure, ρ_{yx}^T depends nonmonotonically on E_F, with a maximum near the threshold and decreasing at a larger E_F. The magnitude of ρ_{yx}^T near the threshold is controlled by skyrmion size a. As the spin-chirality driven mechanism relevant for a small skyrmion size does not work at $E_F < \Delta/2$ (there is no spin-flip processes below the spin down subband edge), the decrease of a (and hence $\beta_{\rm ex}$) suppresses ρ_{yx}^T at $E_F = \Delta/2$. The suppression of ρ_{yx}^T at a large E_F occurs from the one hand due to decrease of the spin polarization factor P_s in ρ_a, and from the other hand due to decrease of the scattering cross section as the kinetic energy of the scattering electron exceeds the characteristic energy of the scattering potential (provided that $\lambda_a \lesssim 1$) [44].

The variation of the Fermi energy affects the asymmetric part of the scattering cross section simultaneously through ka and λ_a factors and, therefore, gives rise to a number of interesting features in the transverse resistivity behavior. We demonstrate these peculiarities in Fig. 7, where the dependence of ρ_{yx}^T, ρ_c, and ρ_a on E_F is plotted for $\beta_{\rm ex} = 3$ and $\beta_{\rm ex} = 6$. For $\beta_{\rm ex} = 3$ [Fig. 7(a)] the adiabatic term ρ_a is

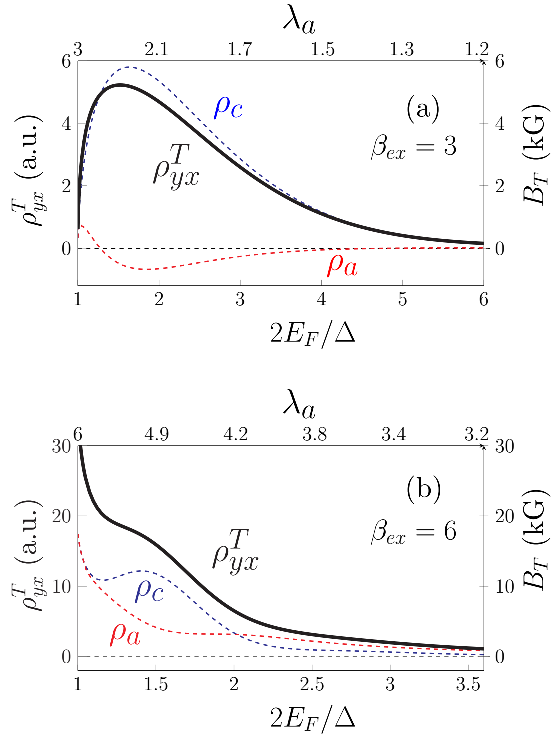

FIG. 7. The dependence of ρ^T_{yx}, ρ_c, ρ_a on Fermi energy E_F at $\beta_{\rm ex} = 3$ (a) and $\beta_{\rm ex} = 6$ (b) for Λ_1 profile, $n_{\rm sk} = 2 \times 10^{11}$ cm^{-2}.

negative when far from the threshold. This is due to the complex scattering pattern typical for the intermediate range of the adiabatic parameter values ($1 \leqslant \lambda_a \leqslant 2$). We have already encountered this effect considering the behavior of THE in the crossover regime: ρ_a is negative in Fig. 2 for the same range of λ_a as in Fig. 7(a). For $\beta_{\rm ex} = 6$ [Fig. 7(b)] λ_a is larger and the interference in the carrier scattering manifests itself through the oscillation of ρ_c, ρ_a magnitudes superimposed on the global suppression upon increasing of E_F. The same oscillating peculiarities of transverse response can be seen in Fig. 2 in the range $4 \leqslant \lambda_a \leqslant 5$.

Let us finally comment on the scattering rates behavior in the vicinity of the threshold $E_F \approx \Delta/2$. Since the spin down and spin-flip scattering channels are absent for $E_F < \Delta/2$, we conclude that at $E_F \approx \Delta/2$ the following relations are fulfilled: $\Gamma_2 \approx 0$, and $\Gamma_1(\theta) \approx \Pi(\theta)$. At that, only spin up scattering channel is activated with $\mathcal{J}_{\uparrow\uparrow} \approx 2\Pi(\theta)$ (i.e., $\rho_a \approx \rho_c$). It is worth mentioning that this relation holds in the vicinity of the threshold for any magnitude of the adiabatic parameter.

B. Dense array of skyrmions

In this section we apply the developed theory of THE to the case when the dominating scattering mechanism changes from scattering on nonmagnetic impurities to scattering on magnetic textures. This transition affects the spin-dependent scattering time $\tau_s^{-1} = \tau_0^{-1} + \omega_s$, and correspondingly the behavior of both the longitudinal and transverse resistivities. Let us consider the adiabatic regime of an electron scattering assuming that the spin-flip scattering channels are completely

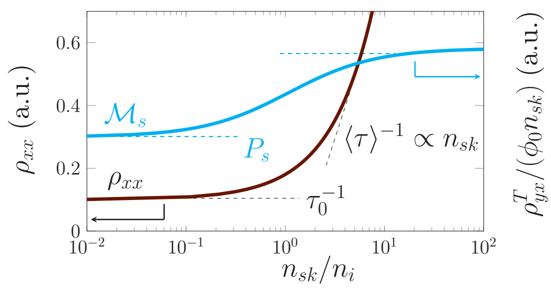

FIG. 8. The dependence of ρ_{xx} and $\mathcal{M}_s$ on skyrmion surface density $n_{\rm sk}$.

suppressed ($\Omega_{\uparrow\downarrow} = \tau_{\uparrow\downarrow}^{-1} = 0$) and THE originates solely from the spin Hall effect ($\rho_a \gg \rho_c$). At that the spin up and spin down channels are uncoupled and contribute independently to the conductivity. While $\Omega_{ss}\tau_0 \ll 1$ in the dilute regime $\omega_s\tau_0 \ll 1$, the ratio $\Omega_{ss}\tau_s \approx \Omega_{ss}/\omega_s$ remains small even in the dense skyrmion system $\omega_s\tau_0 \gg 1$, as the symmetric scattering is more effective than the asymmetric one [57]. Thus, we can still solve the kinetic equation in the lowest order in $\Omega_{ss}\tau_s$ as described in the previous section. Keeping only the leading terms with respect to $\Omega_{ss}\tau_s$ we get for the resistivity tensor (see details in Appendix C):

$$\rho_{xx} = \frac{m}{ne^2\langle\tau\rangle}, \quad \rho^T_{yx} = \mathcal{M}_s \frac{1}{nec}(\phi_0 n_{\rm sk}) \int_0^{2\pi} \Pi \sin\theta d\theta,$$
$$\langle\tau\rangle = \frac{1}{2}[(1+P_s)\tau_\uparrow + (1-P_s)\tau_\downarrow],$$
$$\mathcal{M}_s = \frac{1}{2}\left[(1+P_s)\frac{\tau_\uparrow^2}{\langle\tau\rangle^2} - (1-P_s)\frac{\tau_\downarrow^2}{\langle\tau\rangle^2}\right]. \tag{16}$$

Here $P_s = (n_\uparrow - n_\downarrow)/(n_\uparrow + n_\downarrow)$ is the spin polarization of the 2D free carriers. We have also introduced an averaged scattering time $\langle\tau\rangle$. The parameter $\mathcal{M}_s$ controls the conversion of the spin Hall to the charge Hall current.

In Fig. 8 we plot the dependence of ρ_{xx} and the spin/charge Hall factor $\mathcal{M}_s$ on the skyrmion surface density $n_{\rm sk}$ via the parameter $\omega_s\tau$ covering the transition between scattering on nonmagnetic impurities and skyrmions.

The switching of the dominant scattering mechanism affects the spin dependent scattering time τ_s [Eq. (9)]. In the dilute regime of low skyrmion surface density $\omega_s\tau_0 \ll 1$ considered in the previous section, the total transport scattering time τ_s is independent of the carrier spin, being determined by scattering on host nonmagnetic impurities $\tau_s = \tau_0$. Therefore ρ_{xx} does not depend on $n_{\rm sk}$. Increasing the skyrmion surface density turns the system into the dense skyrmionic regime $\omega_s\tau_0 \gg 1$, when the total transport scattering time is determined solely by the magnetic skyrmions and, hence, depends on the carrier spin state $\tau_s = \omega_s^{-1}$. When ω_s exceeds τ_0^{-1}, the longitudinal resistivity $\rho_{xx} \propto \langle\tau\rangle^{-1}$ increases linearly with $n_{\rm sk}$ as shown in Fig. 8.

According to Eq. (16) the topological Hall resistivity ρ^T_{yx} is proportional to the skyrmion surface density $n_{\rm sk}$. The crossover in the dominating scattering mechanism affects ρ^T_{yx} only via the $\mathcal{M}_s$ factor. In the dilute regime ($\omega_s\tau_0 \ll 1$) this parameter coincides with the carrier spin polarization $\mathcal{M}_s = P_s$ as the scattering time on host impurities τ_0 is spin

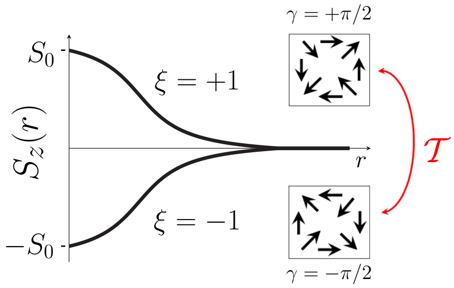

FIG. 9. Two chiral spin textures with opposite orientation $\xi = \pm 1$ and $\varkappa = -1$ connected by the time-inversion $\mathcal{T}$.

independent. However, in the dense regime ($\omega_s \tau_0 \gg 1$) the scattering time τ_s depends on the carrier spin, this dependence creates an additional spin imbalance favoring the conversion of spin to charge currents. As a result, the $\mathcal{M}_s$ factor is renormalized accounting for $\tau_\uparrow \neq \tau_\downarrow$.

The general expressions for ρ_{xx} and ρ_{yx}^T in the adiabatic regime (16) are applicable for any spin-dependent scattering mechanisms, not necessarily due to skyrmions. We point out that in the leading order with respect to $\Omega_{ss}\tau_s$ the effect of τ_s on ρ_{yx}^T can be fully described by the replacement of the carriers spin polarization P_s by an effective $\mathcal{M}_s$ factor, which accounts for $\tau_\uparrow \neq \tau_\downarrow$.

C. Paramagnetic chiral systems

In the previous sections we considered THE in a 2D magnetic layer with a background magnetization S_0 and local deviations forming chiral magnetic textures. Unlike anomalous Hall effect, THE does not necessarily require macroscopic spin polarization of the carriers in the sample. Therefore, THE is allowed in a system with no background magnetization provided it still has localized chiral spin textures. We will refer to this situation as to a chiral paramagnetic case.

In the absence of a preferred magnetization direction the chiral spin textures with opposite orientations can be created in the same sample. We denote them by the orientation of spins in the center $\xi = \mathrm{sgn}(S_z|_{r\to 0}) = \pm 1$. However, these two spin configurations are not independent, they must be connected by the time-inversion symmetry. The example of such a Kramers doublet of spin textures with $\varkappa = -1$ is shown in Fig. 9.

The presence of two spin textures with opposite orientation $\xi = \pm 1$ in the same layer modifies the expression for the charge contribution ρ_c to THE (14). Indeed, as $S_0 \approx 0$ the sign of the spin-chirality driven contributions $\Gamma_{1,2}$ to the carrier asymmetric scattering on the spin texture depends on its orientation and the contributions to ρ_c from textures with $\xi = \pm 1$ have opposite sign. We arrive at the modified expression for ρ_c accounting for both texture orientations $\xi = \pm 1$:

$$\begin{aligned} \rho_c &= P_\xi \frac{1}{nec} (\phi_0 n_{\mathrm{sk}}) \int (\Gamma_1 + \Gamma_2) \sin\theta d\theta, \\ P_\xi &= \frac{n_+ - n_-}{n_+ + n_-}, \end{aligned} \tag{17}$$

where $n_\pm$ are surface densities of $\xi = \pm 1$ spin textures, respectively, $n_{\mathrm{sk}} = n_+ + n_-$ is the total surface density, and P_ξ is the polarization of the texture array in terms of their orientations. Here we consider the dilute regime with $\tau_s = \tau_0$. It follows from (17) that observation of THE in chiral paramagnetic systems is possible only when there is an imbalance in the texture orientations, i.e., $P_\xi \neq 0$.

Let us note that for the positive texture polarization $P_\xi > 0$, the sign of ρ_c is different to that of ρ_c for magnetic skyrmions, or noncollinear rings in Fig. 1. Indeed, as we already mentioned, $\delta S_z < 0$ for the magnetic skyrmions case leading to $\rho_c > 0$. On the contrary, $\delta S_z > 0$ is positive for $\xi = +1$ shown in Fig. 9, so that $\rho_c < 0$.

V. DISCUSSION

Let us summarize the hallmarks of the developed THE theory and consider some of the experimentally studied skyrmion systems. First, the THE contribution to the resistivity $\rho_{yx}^T = \rho_c + \rho_a$ consists of two terms: the first one ρ_c describes the transverse charge current due to spin-independent asymmetric scattering, while the second one ρ_a appears due to spin Hall effect converted to the charge transverse current via nonzero 2DEG spin polarization. Domination of one of the two terms is controlled by the adiabatic parameter λ_a, the crossover from charge Hall dominating to spin Hall dominating regime occurs at $\lambda_a \sim 1$ and is accompanied by a local minimum in the dependence of ρ_{yx}^T on the skyrmion size.

Let us estimate the characteristic values of λ_a for some real skyrmion systems. Skyrmions extensively studied by Panagopoulos' group [16,17,47] in Ir/Fe/Co/Pt multilayers systems are in the range 40–80 nm in size. For an estimate we take [58] $a = 50$ nm, $\Delta = 0.6$ eV, $E_F = 5$ eV, the effective in-plane mass $m = m_0$ and obtain $\lambda_a \approx 30$.

Skyrmions studied by Fert's group [2,3,15] in similar Co/Pt multilayers systems are somewhat larger so that the adiabatic parameter is also in a strong coupling range $\lambda_a \approx 60$. This is also typical for other Co/Pt systems with the size of the skyrmions being around 100 nm [59]. An example of substantially different system is Ta/FeCoB/TaOx structure with skyrmionic bubbles of ~ 1 μm size [60]. The electron transport in such systems is also in the adiabatic regime.

It is worth discussing the role of the ratio $P_s = \Delta/2E_F$ in these systems. According to Fig. 6, ρ_{yx}^T is significantly reduced when $P_s \ll 1$ as discussed in Sec. IV A 4. For the parameters used in the estimation above $P_s \approx 0.06$, thus even at seemingly large skyrmion diameters ρ_{yx}^T can be rather small. Therefore, THE is expected to be more pronounced in systems with higher $\Delta/2E_F$ ratio.

The decrease of λ_a down to the order of unity leading to the nonadiabatic transport regime is expected for nanometer-size chiral magnetic textures in metallic systems with typical ferromagnets such as Co or Fe. In the recent studies of Weisendanger's group a few-nanometer size skyrmions were successfully stabilized [61]. For such nanoscale skyrmions the THE is rather sensitive to band structure parameters, i.e. taking $a = 5$ nm and $P_s = 0.5$ one gets $\lambda_a \approx 30$ so the THE is size-independent [57], while for the smaller ratio of the exchange coupling to the Fermi energy $P_s = 0.06$ one gets $\lambda_a \approx 3$ suggesting that the system is in the vicinity of the crossover from adiabatic to weak coupling regimes.

Alternatively, the nonadiabatic scenario of THE can be achieved in the dilute magnetic semiconductors (DMS). The existence of chiral spin textures in DMS with spin-orbit interaction has been suggested both experimentally [18,19,62] and theoretically on the basis of chiral magnetic polaron [53,56] via the chiral paramagnet scenario discussed in Sec. IV C. The solid advantage of DMS is that both the Fermi energy and the exchange interaction strength can be tuned, allowing us to control the adiabatic parameter in a wide range covering the weak coupling and adiabatic regimes of THE.

For example, taking a n-type $Cd_{1-x}Mn_xTe$-based quantum well (electron effective mass $m \approx 0.1m_0$, the exchange interaction constant $x \times 220$ meV) with a chiral spin texture radius equal to a typical Bohr radius of an impurity bound state 3 nm, for $x = 0.08$ and the electron sheet density $n_1 = 5 \times 10^{11}$ cm^{-2} we get $\lambda_a \approx 2.5$. By decreasing the sheet density down to $n_2 = 1 \times 10^{11}$ cm^{-2} or decreasing Mn fraction down to $x = 0.02$ the adiabatic parameter can be adjusted to $\lambda_a \approx 6$ and $\lambda_a \approx 0.8$, respectively.

Let us comment on material systems where the electron transport is affected by dense array of chiral spin textures. According to the results of Sec. IV B, the THE resistivity in the adiabatic regime $\rho^T_{yx} \propto \mathcal{M}_s(\phi_0 n_{\rm sk})$ linearly depends on the textures surface density, while the coefficient $\mathcal{M}_s$ is renormalized differently depending on whether the carrier scattering is dominated by host impurities or skyrmions. The interplay between the two scattering mechanisms, on the contrary, manifests itself in ρ_{xx}.

One example is a ferromagnetic film in the vicinity of the phase transition, when thermally activated critical magnetic fluctuations lead to the peak in the longitudinal resistivity [28,63–65]. When spin-orbit interaction makes the critical fluctuations chiral a pronounced THE signal is expected, as suggested in Refs. [28,29,65]. Let us mention that to describe the scaling properties of the resistivities $\rho_{yx}(\rho_{xx})$ in the vicinity of FM transition one should specify a specific model of the chiral fluctuations adequate for the considered material system.

ACKNOWLEDGMENTS

We thank M. Chsiev, V. Cross, A. Fert, A. Hallal, H. Jaffres, W. Legrand, D. Maccariello, C. Panagopoulos, M. Raju, and N. Reyren for very fruitful discussions and comments. The work has been carried out under the financial support of Grants from the Russian Science Foundation (asymmetric scattering theory - Project No. 17-12-01182; numerical calculations - Project No. 17-12-01265) and from Russian Foundation of Basic Research (Grant 18-02-00668). It was also supported by the Academy of Finland Grant No. 318500. K.S.D. and N.S.A. thank the Foundation for the Advancement of Theoretical Physics and Mathematics "BASIS."

APPENDIX A: INTEGRATION OF THE COLLISION INTEGRAL AND THE BOLTZMANN EQUATION

In this Appendix we calculate the collision integral in Eq. (3) and derive the system of equations Eq. (8) for the function $g_s^{\pm}$ from Eq. (6). We start from the collision integral

$$\mathrm{St}[g_s(\boldsymbol{p})] = \sum_{\boldsymbol{p}',s'} \big(\mathcal{W}^{ss'}_{\boldsymbol{pp}'} g_{s'}(\boldsymbol{p}') - \mathcal{W}^{s's}_{\boldsymbol{p}'\boldsymbol{p}} g_s(\boldsymbol{p})\big), \quad \text{(A1)}$$

where $g_s(\boldsymbol{p})$ is a nonequilibrium part of the full distribution function. The angular asymmetry of the transport responsible for THE arises from a complex dependence of $g_s(\boldsymbol{p})$ on the polar angle of the momentum $\boldsymbol{p} = (p, \varphi)$, thus in what follows we denote this dependence explicitly as $g_s(\varphi)$. Let us write the scattering rates $\mathcal{W}^{ss'}_{\boldsymbol{pp}'}$ in the form

$$\mathcal{W}^{ss'}_{\boldsymbol{pp}'} = \frac{1}{\nu}\mathcal{A}_{ss'}(\theta)\delta\big(\varepsilon^s_p - \varepsilon^{s'}_{p'}\big),$$
$$\mathcal{A}_{ss'}(\theta) = \frac{2\pi}{\hbar}\nu\big(n_i|u_{\boldsymbol{pp}'}|^2\delta_{ss'} + n_{\rm sk}\big|T^{ss'}_{\boldsymbol{pp}'}\big|^2\big), \quad \text{(A2)}$$

where $\theta = \varphi - \varphi'$ is the scattering angle, δ is the delta function, and $\nu = m/2\pi\hbar^2$ is the 2D density of states, we omit the dependence of $\mathcal{A}_{ss'}$ on the electron energy ε. After integrating Eq. (A1) over ε we arrive at

$$\mathrm{St}[g_s(\varphi)] = \sum_{s'} \int \frac{d\varphi'}{2\pi}(\mathcal{A}_{ss'}(\theta)g_{s'}(\varphi') - \mathcal{A}_{s's}(-\theta)g_s(\varphi)). \quad \text{(A3)}$$

The next step is to expand $g_s(\varphi)$ and $\mathcal{A}_{ss'}(\theta)$ in angular harmonics:

$$g_s(\varphi) = \sum_{n\geqslant 1} g^+_{s,n}\cos n\varphi + g^-_{s,n}\sin n\varphi,$$
$$\mathcal{A}_{ss'}(\theta) = \ell_{0,ss'} + 2\sum_{n\geqslant 1} \ell^+_{n,ss'}\cos n\theta + \ell^-_{n,ss'}\sin n\theta, \quad \text{(A4)}$$

where

$$\ell^+_{n,ss'} = \frac{2\pi}{\hbar}\nu\int_0^{2\pi}\frac{d\theta}{2\pi}\cos n\theta\big(n_i|u_{\boldsymbol{pp}'}|^2\delta_{ss'} + n_{\rm sk}\big|T^{ss'}_{\boldsymbol{pp}'}\big|^2\big),$$
$$\ell_{0,ss'} = \frac{2\pi}{\hbar}\nu\int_0^{2\pi}\frac{d\theta}{2\pi}\big(n_i|u_{\boldsymbol{pp}'}|^2\delta_{ss'} + n_{\rm sk}\big|T^{ss'}_{\boldsymbol{pp}'}\big|^2\big),$$
$$\ell^-_{n,ss'} = \frac{2\pi}{\hbar}\nu n_{\rm sk}\int_0^{2\pi}\frac{d\theta}{2\pi}\sin n\theta\big|T^{ss'}_{\boldsymbol{pp}'}\big|^2.$$

The terms $\ell^-_{n,ss'}$ mix odd $(-)$ and even $(+)$ angular parts of the nonequilibrium distribution function g_s, hence they are responsible for the asymmetric scattering. In these terms we take into account only the scattering on chiral spin textures (i.e., skew scattering due to host impurities leading to the anomalous Hall effect is neglected). It is especially convenient to write the asymmetric coefficients $\ell^-_{n,ss'}$ using the dimensionless rates $\mathcal{J}_{ss'}(\theta)$ introduced in Eq. (5):

$$\ell^-_{n,ss'} = -\frac{e}{mc}(n_{\rm sk}\phi_0)\int_0^{2\pi}\mathcal{J}_{ss'}(\theta)\sin n\theta d\theta, \quad \text{(A5)}$$

where e is a negative electron charge, and $\phi_0 = hc/|e|$ is the flux quantum. After substituting the expansions Eq. (A4) and integrating it over the angle φ' we arrive at the following expression for the collision integral:

$$\mathrm{St}[g_s(\varphi)] = \sum_n \mathcal{I}^+_{s,n}\cos n\varphi + \mathcal{I}^-_{s,n}\sin n\varphi,$$
$$\mathcal{I}^+_{s,n} = \sum_{s'}[\ell^+_{n,ss'}g^+_{s',n} - \ell^-_{n,ss'}g^-_{s',n} - \ell_{0,s's}g^+_{s,n}],$$
$$\mathcal{I}^-_{s,n} = \sum_{s'}[\ell^+_{n,ss'}g^-_{s',n} + \ell^-_{n,ss'}g^+_{s',n} - \ell_{0,s's}g^-_{s,n}]. \quad \text{(A6)}$$

The number of nonzero angular harmonics $g^{\pm}_{n,s}$ in the Boltzmann equation Eq. (3) is determined by a particular transport scenario. For the considered in this paper linear response on the electric field $\boldsymbol{E}$, the field-driven part of Eq. (3) contains only the first angular harmonics $n = 1$; therefore $g^{\pm}_{s,n} = 0$, $\mathcal{I}^{\pm}_{s,n} = 0$ for $n \geqslant 2$, and only the index $n = 1$ is relevant, so we simplify the notation [see Eq. (6)] $g^{\pm}_s \equiv g^{\pm}_{1,s}$. The terms of the collision integral for $n = 1$ are given by

$$\begin{aligned}\mathcal{I}^{+}_{s,1} &= -\tau_s^{-1} g^{+}_s + \Omega_{ss} g^{-}_s + \tau_{s\bar{s}} g^{+}_{\bar{s}} + \Omega_{s\bar{s}} g^{-}_{\bar{s}},\\ \mathcal{I}^{-}_{s,1} &= -\tau_s^{-1} g^{-}_s - \Omega_{ss} g^{+}_s + \tau_{s\bar{s}} g^{-}_{\bar{s}} - \Omega_{s\bar{s}} g^{+}_{\bar{s}},\end{aligned} \tag{A7}$$

where we introduced $\tau_s^{-1} = \ell_{0,ss} - \ell^{+}_{1,ss} + \ell_{0,\bar{s}s}$, $\Omega_{ss'} = -\ell^{-}_{1,ss'}$, and $\tau^{-1}_{s\bar{s}} = \ell^{+}_{1,s\bar{s}}$; $\bar{s}$ denotes the spin state opposite to s. The detailed expressions for τ_s, $\tau_{s\bar{s}}$, $\Omega_{ss'}$ parameters are given in Eq. (9). Assuming that $\boldsymbol{E}$ is directed along the x axis the Boltzmann equation for s spin subband is given by

$$eEv_s \frac{\partial f^0_s}{\partial \varepsilon} \cos\varphi = \mathcal{I}^{+}_{s,1}\cos\varphi + \mathcal{I}^{-}_{s,1}\sin\varphi. \tag{A8}$$

Equating $eEv_s \frac{\partial f^0_s}{\partial \varepsilon} = \mathcal{I}^{+}_{s,1}$, and $\mathcal{I}^{-}_{s,1} = 0$ brings us to the system of algebraic equations Eq. (8) for $g^{\pm}_{1,s}$.

APPENDIX B: SYMMETRY OF SCATTERING RATES

In this Appendix we derive the relations (13) for the dimensionless asymmetric scattering rates $\mathcal{J}_{ss'}(\theta,\eta)$. The background polarization $\eta = \mathrm{sgn}(S_0) = \pm 1$ also determines the orientation of spins inside the core of a chiral spin texture. The starting point is the time-reversal invariance, which states that the scattering rate from $(\boldsymbol{p}', s') \to (\boldsymbol{p}, s)$ with a scattering angle $\theta = \varphi - \varphi'$ should be equal to that from $(-\boldsymbol{p}, \bar{s}) \to (-\boldsymbol{p}', \bar{s}')$ with the scattering angle $-\theta$ and reversed polarization of the spin texture $\boldsymbol{S}(\boldsymbol{r}) \to -\boldsymbol{S}(\boldsymbol{r})$ ($\bar{s}$ denotes the carrier spin state opposite to s). The spin texture reversal $\boldsymbol{S}(\boldsymbol{r}) \to -\boldsymbol{S}(\boldsymbol{r})$ implies $\eta \to -\eta$, $\varkappa \to \varkappa$, and $\gamma \to \gamma + \pi$. Collecting these operations together we obtain

$$\mathcal{G}_{ss'}(\theta,\eta) + \mathcal{J}_{ss'}(\theta,\eta) = \mathcal{G}_{\bar{s}'\bar{s}}(-\theta,-\eta) + \mathcal{J}_{\bar{s}'\bar{s}}(-\theta,-\eta). \tag{B1}$$

Taking into account that $\mathcal{G}_{ss'}(\theta,\eta) = \mathcal{G}_{ss'}(-\theta,\eta)$ and $\mathcal{J}_{ss'}(\theta,\eta) = -\mathcal{J}_{ss'}(-\theta,\eta)$ we get that the symmetric and asymmetric scattering rates satisfy

$$\begin{aligned}\mathcal{G}_{ss'}(\theta,\eta) &= \mathcal{G}_{\bar{s}'\bar{s}}(\theta,-\eta),\\ \mathcal{J}_{ss'}(\theta,\eta) &= -\mathcal{J}_{\bar{s}'\bar{s}}(\theta,-\eta).\end{aligned} \tag{B2}$$

We further focus on $\mathcal{J}_{ss'}$. The relations (B2) couple the two scattering channels with the opposite spin orientations. For the spin-conserving channels we have

$$\mathcal{J}_{\uparrow\uparrow}(\theta,\eta) = -\mathcal{J}_{\downarrow\downarrow}(\theta,-\eta). \tag{B3}$$

Let us introduce the symmetrized and antisymmetrized combinations of $\mathcal{J}_{\uparrow\uparrow}(\theta,\eta)$, $\mathcal{J}_{\uparrow\uparrow}(\theta,-\eta)$ with respect to η:

$$\begin{aligned}\Gamma(\theta,\eta) &= \tfrac{1}{2}[\mathcal{J}_{\uparrow\uparrow}(\theta,\eta) - \mathcal{J}_{\uparrow\uparrow}(\theta,-\eta)],\\ \Pi(\theta) &= \tfrac{1}{2}[\mathcal{J}_{\uparrow\uparrow}(\theta,\eta) + \mathcal{J}_{\uparrow\uparrow}(\theta,-\eta)].\end{aligned} \tag{B4}$$

Since the background polarization can take only two values $\eta = \pm 1$, the function Π does not depend on η, while $\Gamma(-\eta) = -\Gamma(\eta)$. The dependence of Γ on η can be specified explicitly as $\Gamma(\eta,\theta) \equiv \eta\Gamma_1(\theta)$, where Γ_1 depends only on θ and on the energy of the incident electron.

Expressing the rates of the spin-conserving channels and using the symmetry (B3) we arrive at the relations (13)

$$\begin{aligned}\mathcal{J}_{\uparrow\uparrow}(\theta,\eta) &= \eta\Gamma_1(\theta) + \Pi(\theta),\\ \mathcal{J}_{\downarrow\downarrow}(\theta,\eta) &= \eta\Gamma_1(\theta) - \Pi(\theta).\end{aligned} \tag{B5}$$

As for the spin-flip scattering channels, there is an additional symmetry $\mathcal{J}_{\uparrow\downarrow}(\theta,\eta) = \mathcal{J}_{\downarrow\uparrow}(\theta,\eta)$ as the Hamiltonian is Hermitian, this symmetry leads to the absence of a spin Hall part:

$$\mathcal{J}_{\downarrow\uparrow}(\theta,\eta) = \mathcal{J}_{\uparrow\downarrow}(\theta,\eta) = \eta\Gamma_2(\theta), \tag{B6}$$

where $\Gamma_2(\theta)$ does not depend on η.

APPENDIX C: DERIVATION OF THE RESISTIVITY TENSOR ρ

In this Appendix we solve the system of Eq. (8) and calculate the longitudinal (ρ_{xx}) and transverse (ρ^T_{yx}) resistivities for dilute and dense skyrmion systems [see Eqs. (14) and (16)].

1. Dilute regime

In the dilute regime the scattering is dominated by host nonmagnetic impurities: $\tau_s \approx \tau_0 \ll \omega_s^{-1}, \Omega^{-1}_{ss'}$. In this case the longitudinal component g^{+}_s is determined only by τ_0:

$$g^{+}_s = \tau_0 eEv_s\left(-\frac{\partial f^0_s}{\partial \varepsilon}\right). \tag{C1}$$

The transverse part g^{-}_s in the lowest order in $\Omega_{ss'}\tau_0$ is given by

$$g^{-}_s = -\tau_0[\Omega_{ss}g^{+}_s + \Omega_{s\bar{s}}g^{+}_{\bar{s}}]. \tag{C2}$$

The electric current $\boldsymbol{j}$ calculated according to Eq. (7) appears to be

$$\begin{aligned}&j_x = \sigma_0 E, \quad j_y = \sigma^T_{yx}E, \quad \sigma_0 = \frac{ne^2\tau_0}{m},\\ &\sigma^T_{yx} = -\sigma_0\sum_s \frac{n_s}{n}(\Omega_{ss} + \Omega_{s\bar{s}})\tau_0,\end{aligned} \tag{C3}$$

where $n_s = \nu(E_F + s\Delta)$ is the electron sheet density for the s subband, $n = n_\uparrow + n_\downarrow$ is the total electron sheet density, and $\bar{s}$ denotes the spin state opposite to s. Inverting the conductivity tensor and keeping only the leading terms with respect to $\Omega_{ss'}\tau_0$ we get for the resistivities:

$$\rho_{xx} = \sigma_0^{-1}, \quad \rho^T_{yx} = -\sigma_0^{-2}\sigma^T_{yx} = \rho_c + \rho_a, \tag{C4}$$

where ρ_c, ρ_a are given by Eq. (14).

2. Transport in the adiabatic regime

In the adiabatic regimes the spin-flip scattering on skyrmions is suppressed ($\tau^{-1}_{\uparrow\downarrow} = \Omega_{\uparrow\downarrow} = 0$) and the spin Hall term prevails over the charge one $\Pi \gg \Gamma_{1,2}$. The absence of spin-flip scattering suggests that the two spin subbands in Eq. (8) are uncoupled and contribute independently to the electric current. Below we do not put any restrictions on $\omega_s\tau_0$ assuming that the scattering time can be dominated either by impurities or by skyrmions. The product $\Omega_{ss'}\tau_s \ll 1$ leading to the Hall effect remains small as the asymmetric scattering rates are always smaller than the symmetric ones. Keeping these conditions we get for g_s^+ and g_s^-:

$$g_s^+ = \tau_s e E v_s \left(-\frac{\partial f_s^0}{\partial \varepsilon}\right), \quad g_s^- = -g_s^+(\Omega_s \tau_s). \tag{C5}$$

The electric current in Eq. (7) calculated with $g_s^\pm$ from above is given by

$$\begin{aligned} j_x &= \sigma_{xx} E, \quad j_y = \sigma_{yx}^T E, \\ \sigma_{xx} &= \sigma_\uparrow + \sigma_\downarrow, \quad \sigma_s = \frac{n_s e^2 \tau_s}{m}, \\ \sigma_{yx}^T &= -(\sigma_\uparrow \Omega \tau_\uparrow - \sigma_\downarrow \Omega \tau_\downarrow), \end{aligned} \tag{C6}$$

where we take into account $\Omega \equiv \Omega_{\uparrow\uparrow} = -\Omega_{\downarrow\downarrow}$ for the adiabatic scattering regime. The resistivities ρ_{xx}, ρ_{yx}^T in the lowest order of $\Omega\tau_s$ are given by

$$\begin{aligned} \rho_{xx} &= \sigma_{xx}^{-1} = \frac{m}{ne^2}\frac{1}{\langle\tau\rangle}, \quad \langle\tau\rangle = \frac{n_\uparrow}{n}\tau_\uparrow + \frac{n_\downarrow}{n}\tau_\downarrow, \\ \rho_{yx}^T &= -\sigma_{xx}^{-2}\sigma_{yx}^T = \frac{m}{ne^2}\mathcal{M}_s \Omega, \\ \mathcal{M}_s &= \left[\frac{n_\uparrow}{n}\frac{\tau_\uparrow^2}{\langle\tau\rangle^2} - \frac{n_\downarrow}{n}\frac{\tau_\downarrow^2}{\langle\tau\rangle^2}\right], \end{aligned} \tag{C7}$$

where we introduced the parameters $\langle\tau\rangle$, $\mathcal{M}_s$ following the notations in Eq. (16). Taking into account that $n_s/n = (1 + s\Delta/E_F)/2$ we arrive at the expressions for ρ_{xx}, ρ_{yx}^T in the form as in Eq. (16).

[1] N. Nagaosa and Y. Tokura, Nat. Nanotechnoloy **8**, 899 (2013).
[2] A. Fert, V. Cros, and J. Sampaio, Nat. Nanotechnol. **8**, 152 (2013).
[3] A. Fert, N. Reyren, and V. Cros, Nat. Rev. Mater. **2**, 17031 (2017).
[4] R. Wiesendanger, Nat. Rev. Mater. **1**, 16044 (2016).
[5] A. Neubauer, C. Pfleiderer, B. Binz, A. Rosch, R. Ritz, P. G. Niklowitz, and P. Böni, Phys. Rev. Lett. **102**, 186602 (2009).
[6] C. S. Spencer, J. Gayles, N. A. Porter, S. Sugimoto, Z. Aslam, C. J. Kinane, T. R. Charlton, F. Freimuth, S. Chadov, S. Langridge *et al.*, Phys. Rev. B **97**, 214406 (2018).
[7] Y. Li, N. Kanazawa, X. Z. Yu, A. Tsukazaki, M. Kawasaki, M. Ichikawa, X. F. Jin, F. Kagawa, and Y. Tokura, Phys. Rev. Lett. **110**, 117202 (2013).
[8] B. J. Chapman, M. G. Grossnickle, T. Wolf, and M. Lee, Phys. Rev. B **88**, 214406 (2013).
[9] C. Sürgers, G. Fischer, P. Winkel, and H. v. Löhneysen, Nat. Commun. **5**, 3400 (2014).
[10] B. Ueland, C. Miclea, Y. Kato, O. Ayala-Valenzuela, R. McDonald, R. Okazaki, P. Tobash, M. Torrez, F. Ronning, R. Movshovich *et al.*, Nat. Commun. **3**, 1067 (2012).
[11] F. W. Fabris, P. Pureur, J. Schaf, V. N. Vieira, and I. A. Campbell, Phys. Rev. B **74**, 214201 (2006).
[12] T. Taniguchi, K. Yamanaka, H. Sumioka, T. Yamazaki, Y. Tabata, and S. Kawarazaki, Phys. Rev. Lett. **93**, 246605 (2004).
[13] Y. Ohuchi, Y. Kozuka, M. Uchida, K. Ueno, A. Tsukazaki, and M. Kawasaki, Phys. Rev. B **91**, 245115 (2015).
[14] K. Ahadi, L. Galletti, and S. Stemmer, Appl. Phys. Lett. **111**, 172403 (2017).
[15] D. Maccariello, W. Legrand, N. Reyren, K. Garcia, K. Bouzehouane, S. Collin, V. Cros, and A. Fert, Nat. Nanotechnol. **13**, 233 (2018).
[16] A. Soumyanarayanan, M. Raju, A. G. Oyarce, A. K. Tan, M.-Y. Im, A. P. Petrović, P. Ho, K. Khoo, M. Tran, C. Gan *et al.*, Nat. Mater. **16**, 898 (2017).
[17] M. Raju, A. Yagil, A. Soumyanarayanan, A. K. C. Tan, A. Almoalem, O. M. Auslaender, and C. Panagopoulos, arXiv:1708.04084.
[18] L. N. Oveshnikov, V. A. Kulbachinskii, A. B. Davydov, B. A. Aronzon, I. V. Rozhansky, N. S. Averkiev, K. I. Kugel, and V. Tripathi, Sci. Rep. **5**, 17158 (2015).
[19] C. Liu, Y. Zang, W. Ruan, Y. Gong, K. He, X. Ma, Q.-K. Xue, and Y. Wang, Phys. Rev. Lett. **119**, 176809 (2017).
[20] N. Kanazawa, M. Kubota, A. Tsukazaki, Y. Kozuka, K. S. Takahashi, M. Kawasaki, M. Ichikawa, F. Kagawa, and Y. Tokura, Phys. Rev. B **91**, 041122 (2015).
[21] M. Leroux, M. J. Stolt, S. Jin, D. V. Pete, C. Reichhardt, B. Maiorov, Sci. Rep. **8**, 15510 (2018).
[22] P. Bruno, V. K. Dugaev, and M. Taillefumier, Phys. Rev. Lett. **93**, 096806 (2004).
[23] B. Göbel, A. Mook, J. Henk, and I. Mertig, Phys. Rev. B **95**, 094413 (2017).
[24] K. Hamamoto, M. Ezawa, and N. Nagaosa, Phys. Rev. B **92**, 115417 (2015).
[25] S. Mühlbauer, B. Binz, F. Jonietz, C. Pfleiderer, A. Rosch, A. Neubauer, R. Georgii, and P. Böni, Science **323**, 915 (2009).
[26] W. Münzer, A. Neubauer, T. Adams, S. Mühlbauer, C. Franz, F. Jonietz, R. Georgii, P. Böni, B. Pedersen, M. Schmidt *et al.*, Phys. Rev. B **81**, 041203 (2010).
[27] B. Binz and A. Vishwanath, Phys. B: Condens. Matter **403**, 1336 (2008).
[28] J. Ye, Y. B. Kim, A. J. Millis, B. I. Shraiman, P. Majumdar, and Z. Tešanović, Phys. Rev. Lett. **83**, 3737 (1999).
[29] Y. Lyanda-Geller, S. H. Chun, M. B. Salamon, P. M. Goldbart, P. D. Han, Y. Tomioka, A. Asamitsu, and Y. Tokura, Phys. Rev. B **63**, 184426 (2001).
[30] P. B. Ndiaye, C. A. Akosa, and A. Manchon, Phys. Rev. B **95**, 064426 (2017).
[31] G. Tatara, H. Kohno, J. Shibata, Y. Lemaho, and K.-J. Lee, J. Phys. Soc. Jpn. **76**, 054707 (2007).
[32] S. S.-L. Zhang and O. Heinonen, Phys. Rev. B **97**, 134401 (2018).
[33] Y. Taguchi, Y. Oohara, H. Yoshizawa, N. Nagaosa, and Y. Tokura, Science **291**, 2573 (2001).
[34] G. Yin, Y. Liu, Y. Barlas, J. Zang, and R. K. Lake, Phys. Rev. B **92**, 024411 (2015).
[35] J. Zang, M. Mostovoy, J. H. Han, and N. Nagaosa, Phys. Rev. Lett. **107**, 136804 (2011).
[36] G. Tatara and H. Kawamura, J. Phys. Soc. Jpn. **71**, 2613 (2002).
[37] M. Onoda, G. Tatara, and N. Nagaosa, J. Phys. Soc. Jpn. **73**, 2624 (2004).

[38] K. Nakazawa and H. Kohno, arXiv:1808.04543.

[39] K. Nakazawa, M. Bibes, and H. Kohno, J. Phys. Soc. Jpn. **87**, 033705 (2018).

[40] H. Ishizuka and N. Nagaosa, Sci. Adv. **4**, eaap9962 (2018).

[41] K. S. Denisov, I. V. Rozhansky, N. S. Averkiev, and E. Lähderanta, Phys. Rev. Lett. **117**, 027202 (2016).

[42] K. Nakazawa and H. Kohno, J. Phys. Soc. Jpn. **83**, 073707 (2014).

[43] M. V. Sapozhnikov, S. N. Vdovichev, O. L. Ermolaeva *et al.*, Appl. Phys. Lett. **109**, 042406 (2016).

[44] K. S. Denisov, I. V. Rozhansky, N. S. Averkiev, and E. Lähderanta, Sci. Rep. **7**, 17204 (2017).

[45] I. S. Lobanov, H. Jónsson, and V. M. Uzdin, Phys. Rev. B **94**, 174418 (2016).

[46] C. Moreau-Luchaire, C. Moutafis, N. Reyren, J. Sampaio, C. Vaz, N. Van Horne, K. Bouzehouane, K. Garcia, C. Deranlot, P. Warnicke *et al.*, Nat. Nanotechnol. **11**, 444 (2016).

[47] A. Soumyanarayanan, N. Reyren, A. Fert, and C. Panagopoulos, Nature (London) **539**, 509 (2016).

[48] A. Bogdanov and A. Hubert, J. Magn. Magn. Mater. **138**, 255 (1994).

[49] A. Bogdanov and A. Hubert, J. Magn. Magn. Mater. **195**, 182 (1999).

[50] A. Belavin and A. Polyakov, JETP Lett. **22**, 245 (1975).

[51] L. Brey, Nano Lett. **17**, 7358 (2017).

[52] P. F. Bessarab, G. P. Müller, I. S. Lobanov, F. N. Rybakov, N. S. Kiselev, H. Jónsson, V. M. Uzdin, S. Blügel, L. Bergqvist, and A. Delin, Sci. Rep. **8**, 3433 (2018).

[53] K. Denisov and N. Averkiev, Appl. Phys. Lett. **112**, 162409 (2018).

[54] K. S. Denisov and N. S. Averkiev, JETP Lett. **99**, 400 (2014).

[55] Y. Berkovskaya, B. Gel'mont, and E. Tsidil'kovskii, Sov. Phys. Semicond. **22**, 539 (1998).

[56] Y. Berkovskaya, E. Vakhabova, B. Gel'mont, and I. Merkulov, JETP **67**, 750 (1988).

[57] K. Denisov, I. Rozhansky, M. Potkina, I. Lobanov, E. Lahderanta, and V. Uzdin, arXiv:1803.06124.

[58] M. Chshiev, A. Hallal, and A. Fert (private communication, 2018).

[59] O. Boulle, J. Vogel, H. Yang, S. Pizzini, D. de Souza Chaves, A. Locatelli, T. O. Mentes, A. Sala, L. D. Buda-Prejbeanu, O. Klein *et al.*, Nat. Nanotechnol. **11**, 449 (2016).

[60] T. Srivastava, M. Schott, R. Juge, V. Křižáková, M. Belmeguenai, Y. Roussigné, A. Bernand-Mantel, L. Ranno, S. Pizzini, S.-M. Chérif *et al.*, Nano Lett. **18**, 4871 (2018).

[61] P.-J. Hsu, L. Rózsa, A. Finco, L. Schmidt, K. Palotás, E. Vedmedenko, L. Udvardi, L. Szunyogh, A. Kubetzka, K. von Bergmann *et al.*, Nat. Commun. **9**, 1571 (2018).

[62] D. R. Yakovlev and W. Ossau, in *Introduction to the Physics of Diluted Magnetic Semiconductors* (Springer, Berlin, 2010), pp. 221–262.

[63] L. W. Shacklette, Phys. Rev. B **9**, 3789 (1974).

[64] M. Wang, R. Marshall, K. Edmonds, A. Rushforth, R. Campion, and B. Gallagher, Appl. Phys. Lett. **104**, 132406 (2014).

[65] L. Oveshnikov and E. Nekhaeva, Semiconductors **51**, 1313 (2017).